wake; $N = 7$); a principal component analysis was then applied. Significance of the extracted component vector was assessed by using permutation tests [B. F. J. Manly, *Randomization and Monte Carlo Methods in Biology* (Chapman & Hall, New York, 1990)] by randomly permuting the sign of data entries 19 times; P values were derived by determining the proportion of permuted trials with higher first eigenvalues than the original data. Stability of regional loadings was assessed by the bootstrap procedure [B. Efron, *SIAM Monogr.* **38-I** (1982)]. Fit values of the original loadings across 10,000 bootstrap samples, expressed as Z-scores, were calculated; absolute values > 2.4 were considered stable.
13. Cluster 1, left hemisphere: 8688 mm^3; P' ($n_{max} > k$), corrected = 7.90×10^{-4}; centered $x = -4.9$, $y = -67.9$, $z = -5.3$; cluster 2, right hemisphere: 21056 mm^3; P' ($n_{max} > k$), corrected = 2.14×10^{-7}; centered $x = 21.9$, $y = -51.8$, $z = -6.8$.
14. S. M. Kosslyn and K. N. Ochsner, *Trends Neurosci.* **17**, 290 (1994).
15. A. Rechtschaffen, P. Verdone, J. Wheaton, *Can. Psychiatr. Assoc. J.* **8**, 409 (1963).
16. 17427 mm^3; P' ($n_{max} > k$), corrected = 1.90×10^{-6}; centered $x = 2.8$, $y = -83.0$, $z = 0.4$.
17. Absolute PCO_2 corrected flow rates were consistently lower during REM sleep than during SWS throughout the striate cortex [ΔrCBF = -6.40 ± 5.9 ml/100 g/min (mean ± SD), $x = 4$, $y = -82$, $z = 0$], and absolute rCBF rates were consistently elevated in extrastriate regions (in the fusiform cortex, ΔrCBF = $+8.85 \pm 2.79$ ml/100 g/min, $x = -34$, $y = -56$, $z = -8$), although variances in absolute values were large.
18. 58320 mm^3; P' ($n_{max} > k$), corrected = 3.55E −15; centered $x = -3.9$, $y = 0.3$, $z = 1.2$.
19. D. A. Chavis and D. N. Pandya, *Trans. Am. Neurol. Assoc.* **99**, 192 (1974); W. A. Suzuki and D. G. Amaral, *J. Comp. Neurol.* **350**, 497 (1994).
20. The frontal eye fields (superior dorsolateral prefrontal and premotor cortices) were incompletely sampled in many subjects and are not included in this analysis.
21. The bootstrapping procedures indicated that most regional loadings were stable. In the REM-SWS contrast, all the fusiform-inferotemporal regions—but none of the lateral occipital regions—were associated with Z-scores exceeding threshold (local maximum = 5.44, $x = \pm 48$, $y = -62$, $z = 0$). In the REM-wake contrast, six of the seven fusiform-inferotemporal regions (maximum 4.18, $x = \pm 48$, $y = -62$, $z = 4$), and four of the six lateral occipital regions (maximum 3.58, $x = \pm 32$, $y = -86$, $z = 0$) were stable; in the latter case, all were located in ventral rather than dorsal portions of the lateral occipital cortex ($z \leq 8$ mm). In the REM-SWS contrast, five of the seven striate loadings were stable (local minimum = -3.79, $x = \pm 4$, $y = -82$, $z = 0$), and in the REM-wake contrast, six of seven loadings were stable (minimum = -9.89, $x = \pm 4$, $y = -82$, $z = 0$).
22. S. Zeki *et al.*, *J. Neurosci.* **11**, 641 (1991); D. Watson *et al.*, *Cereb. Cortex* **3**, 79 (1993); J. V. Haxby *et al.*, *J. Neurosci.* **14**, 6336 (1994); I. Sereno *et al.*, *Science* **268**, 889 (1995).
23. These results could reflect the central effects of saccadic eye movements per se. Voluntary saccades during wakefulness previously have been found to be associated with reductions in visual CBF [T. Paus, S. Marrett, K. J. Worsley, A. C. Evans, *J. Neurophysiol.* **74**, 2179 (1995)]. However, saccades in that study were continuous and rapid (40 to 140 in 60 s) but were intermittent and lower in frequency in our own study [0 to 11 in 60 s (5.5 ± 4.0, mean ± SD]. Furthermore, reductions in rCBF were more widely distributed throughout the visual cortex, and no positive correlations between extrastriate activity and saccadic eye movements were observed, which suggests that the striate-extrastriate dissociation evident in this study may be a unique characteristic of REM sleep.
24. R. W. McCarley, J. W. Winkelman, F. H. Duffy, *Brain Res.* **274**, 359 (1983); C. W. Callaway, R. Lydic, H. A. Baghdoyan, J. A. Hobson, *Cell Mol. Neurobiol.* **7**, 105 (1987).
25. The effects of the PGO wave generator on the occipital cortex do not appear to be mediated through the lateral geniculate nucleus [J. A. Hobson, J. Alexander, C. J. Frederickson, *Brain Res.* **14**, 607 (1969)] and therefore are not expected to be exclusively associated with striate projections. Early studies also demonstrated that PGO wave amplitudes in the lateral association areas of the cat visual cortex exceed those in primary visual cortices [D. C. Brooks, *Exp. Neurol.* **22**, 603 (1968)], and single unit studies have shown that the facilitatory effects of PGO waves on neuronal firing rates appear to be manifest in extrastriate but not in striate cortices [T. Kasamatsu and W. R. Adey, *Brain Res.* **55**, 323 (1973)].
26. D. R. Goodenough, H. B. Lewis, A. Shapiro, I. Sleser, *J. Nerv. Ment. Dis.* **140**, 365 (1965); P. Verdone, *Percept. Mot. Skills* **20**, 1253 (1965); T. Pivik and D. Foulkes, *Science* **153**, 1282 (1966); W. Dement and E. A. Wolpert, *J. Exp. Psychol.* **55**, 543 (1958). See also (*2, 14*).
27. This appears to be consistent with the finding of Roland and Gulyas (*3*). However, our results may not be directly comparable with studies of conscious visual imagery; task-elicited activation of the primary visual cortex seen by Kosslyn *et al.* (*4*) might be a special feature of conscious visual imagery or retrieval processes that occur during the waking state.
28. P. Maquet *et al.* [*Nature* **383**, 163 (1996)] did not list rCBF changes in visual cortices; however, they compared REM sleep with an amalgam of wake and non-REM stages, whereas our contrasts were stage specific (for example, REM-SWS) and may be more sensitive.
29. P. L. Madsen *et al.* [*J. Cereb. Blood Flow Metab.* **11**, 502 (1991)] reported REM-associated increases in rCBF in visual association cortices; functional relationships between activity in striate and extrastriate cortices were not evaluated.
30. C. C. Hong *et al.* [*Sleep* **18**, 570 (1995)] reported a positive correlation between REM density and glucose metabolic rates in lateral occipital cortex, but results for primary visual cortex were not reported.
31. S. Zeki, *A Vision of the Brain* (Blackwell, Oxford, 1993). See also (*3, 4*).
32. A pattern of extrastriate activity in the absence of striate function also characterizes clinical states associated with unusual and often bizarre perturbations of visual awareness, such as blindsight [L. Weiskrantz, J. L. Barbur, A. Sahraie, *Proc. Natl. Acad. Sci. U.S.A.* **92**, 6122 (1995)] and confabulatory denial of blindness [G. Goldenberg, W. Mullbacher, A. Nowak, *Neuropsychologia* **33**, 1373 (1995)]. The features of both syndromes suggest that synchronous activation of primary and extrastriate cortices may be essential for "normal" visual awareness. That such coherence appears to be breached during REM sleep is not inconsistent with the altered awareness that characterizes this sleep stage.
33. Decreases in activity in the prefrontal cortex during REM sleep have been noted previously by Madsen *et al.* (*29*) and by Maquet *et al.* (*28*). On the other hand, Hong *et al.* (*30*) reported positive correlations between REM density and absolute glucose metabolic rates in the (right) dorsolateral prefrontal cortex; however, this measure, which reflects physiological responses over a longer time period, may not be directly comparable with normalized rCBF values evaluated in this study.
34. A. Rechtschaffen, *Sleep* **1**, 97 (1978); J. A. Hobson, *Endeavour* **20**, 86 (1996).
35. The authors wish to thank Dr. Alex Martin for his expertise, insight, and critical suggestions, which were essential in the preparation of this manuscript, and Dr. Scott Selbie for his valuable help in preparing Fig. 1.

11 August 1997; accepted 18 November 1997

Discrete Start Sites for DNA Synthesis in the Yeast *ARS1* Origin

Anja-Katrin Bielinsky and Susan A. Gerbi*

Sites of DNA synthesis initiation have been detected at the nucleotide level in a yeast origin of bidirectional replication with the use of replication initiation point mapping. The *ARS1* origin of *Saccharomyces cerevisiae* showed a transition from discontinuous to continuous DNA synthesis in an 18–base pair region (nucleotides 828 to 845) from within element B1 toward B2, adjacent to the binding site for the origin recognition complex, the putative initiator protein.

An origin of bidirectional DNA replication is characterized by the transition between continuous DNA synthesis (proceeding in one direction) and discontinuous synthesis (proceeding in the opposite direction). We have developed replication initiation point (RIP) mapping to determine this transition in the autonomously replicating sequence (ARS) 1 of the yeast *Saccharomyces cerevisiae*.

ARS1 functions as an origin of DNA replication (ORI) both on a plasmid and in its normal context on chromosome IV (*1*). *ARS1*-containing plasmids respond normally to the cell cycle, duplicating once per cycle (*2*), and replication is initiated by the same cellular protein machinery acting on chromosomes.

ARS1 is composed of subdomains A, B1, B2, and B3 (*3*). Subdomains A and B1 are recognized by the origin recognition complex (ORC) (*4*), the putative initiator protein (*5*) indispensable for origin function (*6, 7*). Element B2 is easily unwound DNA (*8*) and element B3 is a binding site for the ARS binding factor I (ABFI) (*9*).

RIP mapping, described here, has sufficient sensitivity for study of eukaryotic origins, unlike an earlier method (*10*). It allows precise mapping of initiation sites for DNA synthesis and was applied to a

Department of Molecular Biology, Cell Biology and Biochemistry, Division of Biology and Medicine, Brown University, Providence, RI 02912, USA.

* To whom correspondence should be addressed. E-mail: susan_gerbi@brown.edu

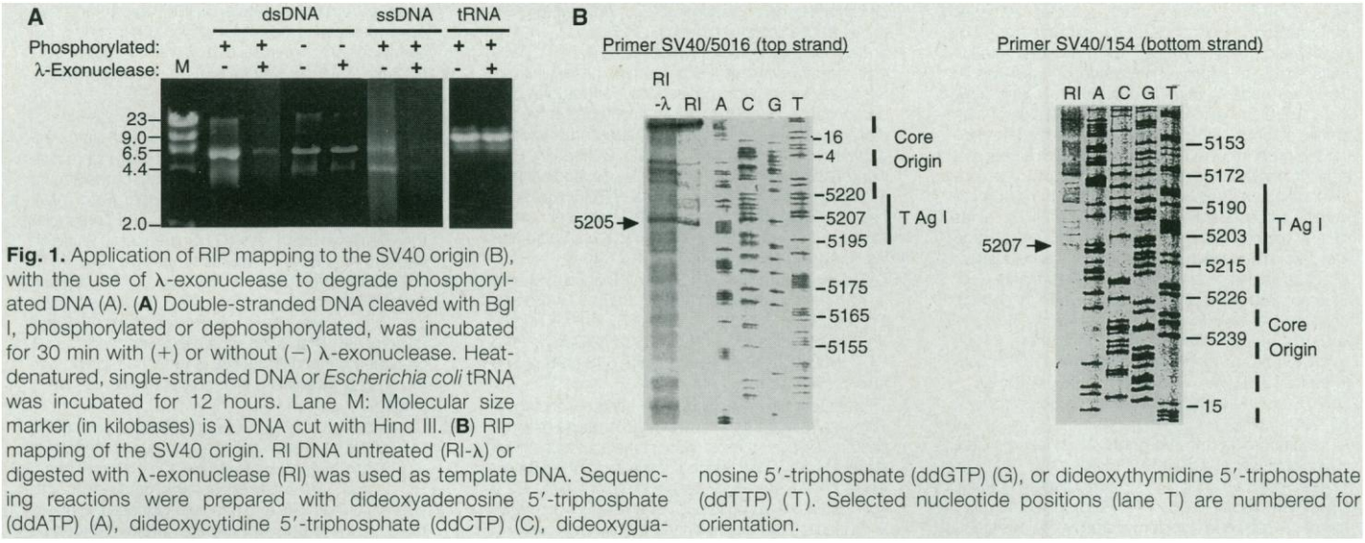

Fig. 1. Application of RIP mapping to the SV40 origin (B), with the use of λ-exonuclease to degrade phosphorylated DNA (A). (**A**) Double-stranded DNA cleaved with Bgl I, phosphorylated or dephosphorylated, was incubated for 30 min with (+) or without (−) λ-exonuclease. Heat-denatured, single-stranded DNA or *Escherichia coli* tRNA was incubated for 12 hours. Lane M: Molecular size marker (in kilobases) is λ DNA cut with Hind III. (**B**) RIP mapping of the SV40 origin. RI DNA untreated (RI-λ) or digested with λ-exonuclease (RI) was used as template DNA. Sequencing reactions were prepared with dideoxyadenosine 5′-triphosphate (ddATP) (A), dideoxycytidine 5′-triphosphate (ddCTP) (C), dideoxyguanosine 5′-triphosphate (ddGTP) (G), or dideoxythymidine 5′-triphosphate (ddTTP) (T). Selected nucleotide positions (lane T) are numbered for orientation.

193–base pair (bp) fragment containing yeast *ARS1*. We chose the wild-type *ARS1* construct (pARS1/WTA) transformed into *S. cerevisiae* strain SP1 (approximately two copies per cell), also used for other analyses of origin function (*3*, *11*). Nuclear DNA was isolated from asynchronously growing cultures, and replicative intermediate (RI) DNA was enriched by benzoylated naphthoylated DEAE (BND) cellulose column chromatography (*12*). RI DNA was treated with λ-exonuclease to eliminate nicked DNA (*12*) (Fig. 1A). Nascent DNA strands with an attached RNA primer are resistant to λ-exonuclease digestion (*13*) and were subsequently used as template DNA to extend a primer to the junction with the RNA primer.

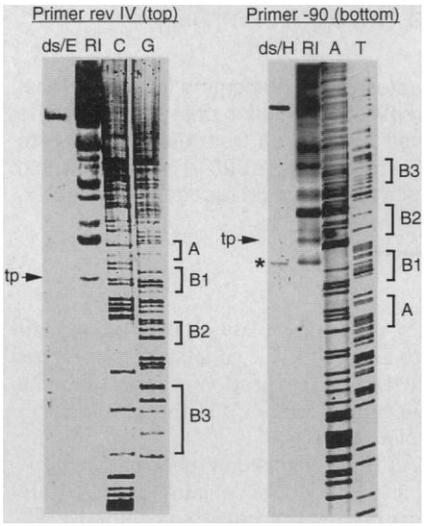

Fig. 2. RIP mapping of the yeast *ARS1* origin. (**A**) Analysis of the top and (**B**) bottom strand. RI DNA from SP1/p*ARS1*/WTA digested with λ-exonuclease was used as template DNA. Double-stranded, nonreplicating yeast DNA cleaved with Eco RI (ds/E) or Hind III (ds/H) served as a control. Sequencing reactions with ddATP (A), ddCTP (C), ddGTP (G), or ddTTP (T) are shown. The position of a polymerase pause site at nt 845 seen with primer −90 is indicated by an asterisk. tp, transition point.

RIP mapping of simian virus (SV) 40 ORI (Fig. 1B) indicates essentially the same start sites as those previously identified by a different method (*10*). Multiple individual 5′ DNA ends represent multiple start sites for SV40 DNA synthesis. Blank areas on the gel reflect regions of continuous DNA synthesis. The nucleotide position at the 5′ end of the smallest detectable fragment marks the transition point between discontinuous and continuous DNA synthesis (Fig. 1B) and thus the site of leading strand initiation.

RIP mapping was next used to analyze *ARS1*. To demonstrate that the primers annealed specifically, we used double-stranded nonreplicating DNA (dsDNA) cleaved at a unique restriction site as the template for primer extension to the restriction site (Fig. 2). No endogenous pause sites were detected for primer extension on the top strand. However, when the bottom strand was analyzed, a second fragment sometimes appeared that we interpreted as an endogenous pause site because the band also occurred when the yeast *ARS1* plasmid was replicated in bacteria, indicating that it was not linked to the replication process in yeast (*14*). When nascent DNA was analyzed with primers rev IV and −90 (Fig. 2, lanes RI), which annealed 100 nucleotides (nt) beyond the left and right borders of *ARS1*, respectively, multiple individual start sites for DNA synthesis were detected with a distinct transition from discontinuous to continuous initiation. We confirmed the start sites mapped on each strand using different primers (*14*). Thus, within the 400-bp region containing *ARS1* and adjacent vector sequences, the transition point for the top strand mapped to nt 845 and for the bottom strand to nt 828 (Fig. 3B). Hence, there is an 18-bp transition region (including the bands at each end), which partly overlaps the ORC binding site. The polyomavirus origin also shows a transition zone of 18 bp (*15*), but the SV40 origin transition occurs within 2 to 3 nt (*10*) (Fig. 3A).

Additional evidence that the initiation sites we observed were linked to the process of replication was provided by analyzing nascent strands derived from an inactive copy of *ARS1*, carrying a mutation in element A, that is replicated through function of an active wild-type *ARS1* on the same plasmid (*16*). If replication forks generated by the wild-type *ARS1* origin proceed at the same rates in both directions, they should meet at approximately nt 2900 of the construct pARS/A$^-$&WT (Fig. 4A). DNA replication through the inactive *ARS1*/A$^-$ would be discontinuous on the bottom strand and continuous on the top strand. The replication initiation point patterns determined by RIP mapping were consistent with this model (Fig. 4B, lanes A$^-$). No primer extension products smaller than several kilobases were detected on the top strand, whereas multiple start sites were observed throughout *ARS1*/A$^-$ on the bottom strand (Fig. 4B).

The distance between *ARS1* sites most frequently used (longest arrows in Fig. 3B) was ~20 to 50 nt. However, Okazaki fragments in higher eukaryotes average over 100 nt (*17*, *18*). We analyzed the length of nascent strands with intact bi- or triphosphorylated RNA primers in a labeling reaction with the RNA-specific "capping enzyme" guanylyltransferase (*19*). Labeled fragments of 20 to 35, 40 to 50, 60, 70 to 80,

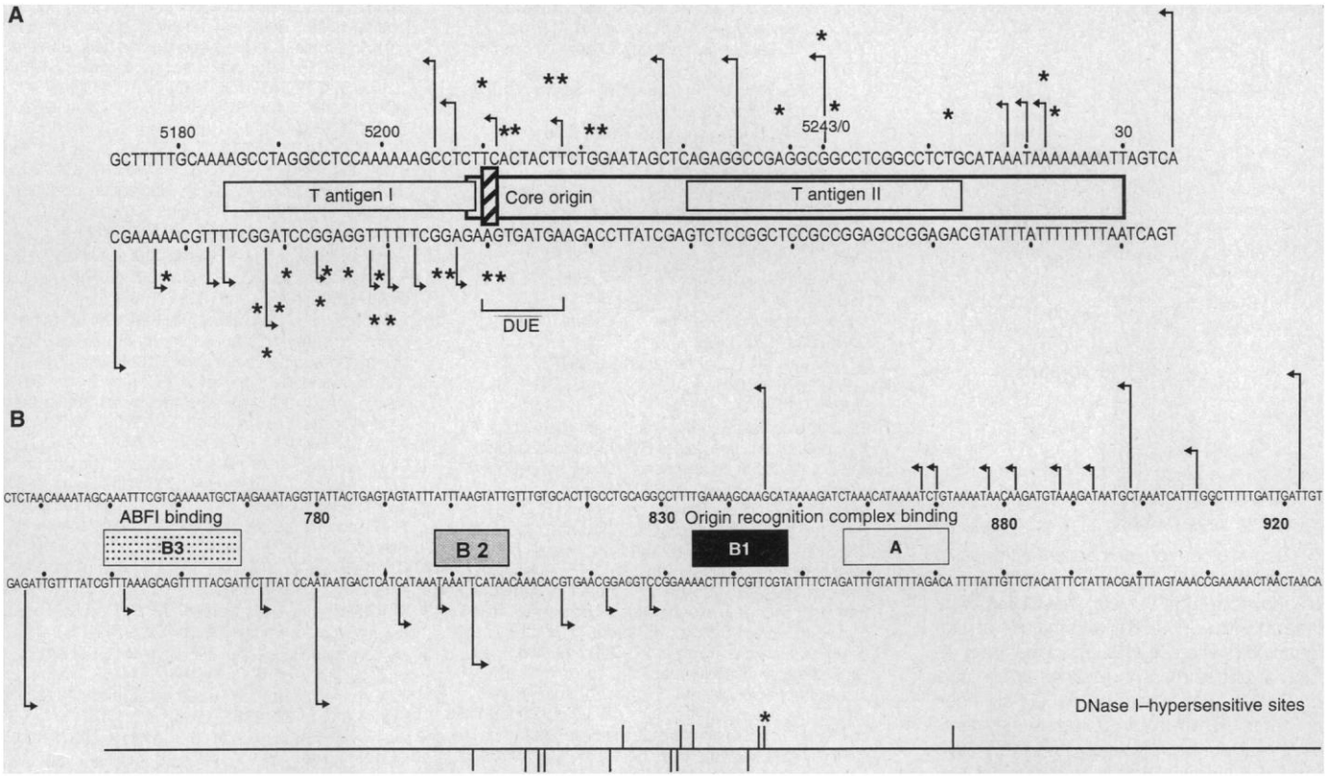

Fig. 3. Map of start sites detected for DNA synthesis. DNA 5′ ends detected as start sites for DNA synthesis in this study are indicated by arrows. Stronger bands on the gels are shown by longer arrows and weaker bands by shorter arrows. (**A**) SV40 origin (*10*). The striped bar and asterisks indicate the transition point and DNA start sites, respectively, previously mapped by Hay and DePamphilis (*10*). DUE, DNA unwinding element. (**B**) Yeast *ARS1*. DNase I–hypersensitive sites mapped by genomic footprinting and in vitro (*4*) are shown below the map, with the most pronounced site indicated by an asterisk.

and 125 nt accumulated preferentially (Fig. 5), similar to the size distribution of nascent strands in SV40 DNA (*20*) and *Drosophila* (*21*). Therefore, this seems to be a conserved feature among eukaryotes. Whether this size distribution is due to DNA polymerase δ pauses or reflects a discontinuous mechanism underlying the formation of Okazaki fragments ("discontinuity model") (*20*) remains to be determined.

What accounts for the multiple initiation sites mapped in this study and for SV40 (*10*) and polyomavirus (*15*)? It is likely that most of these sites reflect positions where discontinuous (lagging strand) synthesis initiates, and individual replicating molecules might choose different sites to initiate DNA synthesis, resulting in population polymorphism. However, we cannot determine whether some are alternate start sites for continuous (leading strand) synthesis. Indeed, the primer extension product that maps to the transition point was not the strongest band for the SV40 origin or for yeast *ARS1*, as would have been expected if it represented the only leading strand initiation site used by every replicating molecule.

An origin of bidirectional replication can be defined as a cis-acting sequence upon which the trans-acting replication machinery assembles. An indispensable part of this machinery is the initiator protein (*5*). In SV40 the transition region is close to the binding site for the viral initiator protein, large tumor (T) antigen, and adjacent to a DNA unwinding element (DUE) (*22*) (Fig. 3A). Similarly, the transition region in

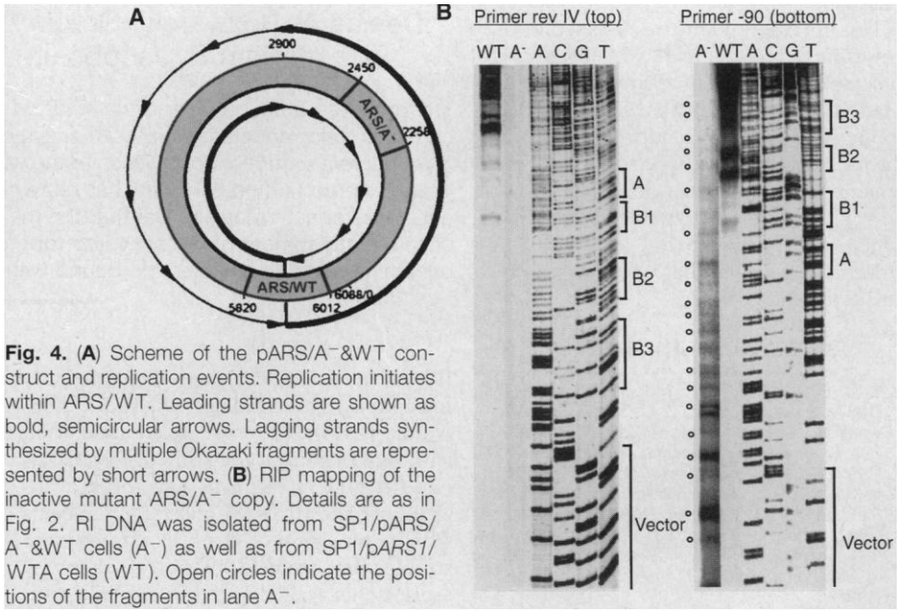

Fig. 4. (**A**) Scheme of the pARS/A⁻&WT construct and replication events. Replication initiates within ARS/WT. Leading strands are shown as bold, semicircular arrows. Lagging strands synthesized by multiple Okazaki fragments are represented by short arrows. (**B**) RIP mapping of the inactive mutant ARS/A⁻ copy. Details are as in Fig. 2. RI DNA was isolated from SP1/pARS/A⁻&WT cells (A⁻) as well as from SP1/p*ARS1*/WTA cells (WT). Open circles indicate the positions of the fragments in lane A⁻.

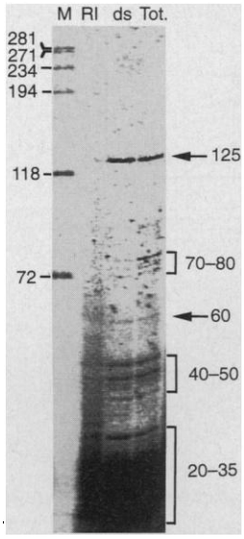

Fig. 5. Size distribution of nascent strands in yeast. (p)ppRNA-DNA chains from RI DNA and dsDNA and from total nuclear yeast DNA were radiolabeled with [α-^{32}P]GTP with the use of vaccinia guanylyltransferase (*19*). The label was removed by alkali treatment, indicating that the label was on RNA primers (*14*). The double-stranded fraction contains "full-length" Okazaki fragments of 125 nt that are not efficiently bound by BND cellulose. "Full-length" Okazaki fragments of 125 nt are absent in RI DNA, as they are already processed or ligated to leading strands. Lane M: Molecular size marker (in bases) is 0X174 RF DNA cut with Hae III.

ARS1 is flanked by the binding site of ORC, the putative initiator protein, and by element B2 (*8*) (Fig. 3B). Mutations in B2 of *ARS1* reduce replication efficiency (*3*), whereas mutations in the transition region, between B1 and B2, do not affect replication efficiency in vivo (*3*). This suggests that the transition region itself has no cis-regulatory function.

The initiation points we detected in the transition region coincide with deoxyribonuclease I–hypersensitive sites that are exposed on each strand of *ARS1* upon ORC binding in vivo and in vitro (*4*) (Fig. 3). The most pronounced hypersensitive site in element B1 (*4*) is at the transition point on the top strand. The coincidence of ORC-induced hypersensitive sites with DNA initiation sites suggests that ORC defines the transition region.

REFERENCES AND NOTES

1. B. J. Brewer and W. L. Fangman, *Cell* **51**, 463 (1987); J. A. Huberman, L. D. Spotila, K. A. Nawotka, S. M. El-Assouli, L. R. Davis, *ibid.*, p. 473; B. J. Brewer and W. L. Fangman, *Bioessays* **13**, 317 (1991); C. S. Newlon, *Microbiol. Rev.* **52**, 568 (1988).
2. V. A. Zakian, B. J. Brewer, W. L. Fangman, *Cell* **17**, 923 (1979); W. L. Fangman, R. H. Hice, E. Chlebowicz Sledziewska, *ibid.* **32**, 831 (1983); R. A. Laskey, M. P. Fairman, J. J. Blow, *Science* **246**, 609 (1989).
3. Y. Marahrens and B. Stillman, *Science* **255**, 817 (1992).
4. S. P. Bell and B. Stillman, *Nature* **357**, 128 (1992); J. F. X. Diffley and J. H. Cocker, *ibid.*, p. 169; J. F. X. Diffley, J. H. Cocker, S. J. Dowell, A. Rowley, *Cell* **78**, 303 (1994).
5. F. Jacob, S. Brenner, F. Cuzin, *Cold Spring Harbor Symp. Quant. Biol.* **28**, 329 (1964).
6. S. P. Bell, R. Kobayashi, B. Stillman, *Science* **262**, 1844 (1993); M. Foss, F. J. McNally, P. Laurenson, J. Rine, *ibid.*, p. 1838; G. Micklem, A. Rowley, J. Harwood, K. Nasmyth, J. F. X. Diffley, *Nature* **366**, 87 (1993); S. Loo *et al.*, *Mol. Biol. Cell* **6**, 741 (1995).
7. C. Liang, M. Weinreich, B. Stillman, *Cell* **81**, 667 (1995).
8. S. Lin and D. Kowalski, *Mol. Cell. Biol.* **17**, 5473 (1997).
9. J. F. X. Diffley and B. Stillman, *Proc. Natl. Acad. Sci. U.S.A.* **85**, 2120 (1988).
10. R. T. Hay and M. L. DePamphilis, *Cell* **28**, 767 (1982).
11. A. Rowley, J. H. Cocker, J. Harwood, J. F. X. Diffley, *EMBO J.* **14**, 2631 (1995).
12. RIP mapping assay on SV40 and yeast nascent DNA was performed as follows. SV40 was propagated and DNA isolated as described (*10*). SP1 yeast cells were transformed with pARS1/WTA (*3*). DNA was isolated and fractionated into dsDNA and RI DNA by BND cellulose chromatography (*7*). About 1 μg of RI DNA was heat-denatured, phosphorylated by T4 polynucleotide kinase with 50 μM adenosine triphosphate (ATP) (*10*), then incubated for 12 hours with 6 to 8 U of λ-exonuclease (Gibco) in 67 mM glycine-KOH (pH 8.8), 2.5 mM $MgCl_2$, and bovine serum albumin (50 μg/ml) at 37°C. The reaction was terminated by incubation at 75°C for 10 min. DNA was extracted once with chloroform–isoamyl alcohol. Primer extension reactions (30 μl) contained 5 ng of SV40 or 500 ng of yeast template DNA (measured by spectrophotometry before the λ-exonuclease treatment), 200 μM nucleoside triphosphates, 125 nM γ-^{32}P–labeled primer with a specific radioactivity of 10^8 cpm/μg, and 2 U of Vent (exo-) DNA polymerase (New England Biolabs) in reaction buffer [10 mM KCl, 10 mM $(NH_4)_2SO_4$, 20 mM tris-HCl (pH 8.8), 13.7 mM $MgSO_4$; modified from C. Santocanale and J. F. X Diffley, *EMBO J.* **15**, 6671 (1996)]. Thirty cycles of 1 min at 95°C, 1 min at 70°C, and 1.5 min at 72°C were performed in a Perkin-Elmer Thermocycler (Gene Amp PCR System 2400). Samples were extracted with chloroform, precipitated with ethanol, and resuspended in 3 μl of 95% formamide loading buffer. Samples were fractionated on 6% polyacrylamide–8 M urea sequencing gels. Primers used for RIP mapping were as follows: SV40/5016, 5′-CTTCATCTCCTCCTTTATCAGGATG-3′ (nt 5016 to 5040); SV40/154, 5′-CAGCAGGCAGAAGTATGCAAAGC-3′ (nt 154 to 131); rev IV, 5′-GCTTCCGGCTCGTATGTTGTGTGG-3′ (nt 617 to 640); and −90, 5′- CTGGCGAAAGGGGGATGTGCTG-3′ (nt 1032 to 1011). Nucleotide positions correspond to those in the maps shown in Fig. 3.
13. C. M. Radding, *J. Mol. Biol.* **18**, 235 (1966).
14. A.-K. Bielinsky and S. A. Gerbi, data not shown.
15. E. A. Hendrickson, C. E. Fritze, W. R. Folk, M. L. DePamphilis, *EMBO J.* **6**, 2011 (1987).
16. We constructed the plasmid pARS/A⁻&WT by cloning a wild-type *ARS1* copy into the Aat II restriction site of the shuttle vector pARS1/858-865 (*3*). The 193-bp wild-type copy of *ARS1* (nt 734 to 926 shown in Fig. 3B) was amplified by annealing the oligonucleotides 5′-ATATATGACGTCACTCTAACAAAATAGCAAATTTC-3′ and 5′-ATATATGACGTCACAATCAATCAAAAAGCCAAA-3′, carrying an Aat II restriction site, to pARS/WTA plasmid DNA and extending them with Taq polymerase. Both ARS1 copies (active and inactive) have the same orientation.
17. S. Anderson, G. Kaufman, M. L. DePamphilis, *Biochemistry* **16**, 4990 (1977).
18. W. C. Burhans, L. T. Vassilev, M. S. Caddle, N. H. Heintz, M. L. DePamphilis, *Cell* **62**, 955 (1990).
19. M. Yamaguchi, E. A. Hendrickson, M. L. DePamphilis, *Mol. Cell. Biol.* **5**, 1170 (1985).
20. T. Nethanel, S. Reisfeld, G. Dinter Gottlieb, G. Kaufmann, *J. Virol.* **62**, 2867 (1988).
21. A. B. Blumenthal and E. J. Clark, *Cell* **12**, 183 (1977).
22. M. L. DePamphilis, *Annu. Rev. Biochem.* **62**, 29 (1993).

23. We thank C. Liang and B. Stillman for advice and yeast ARS clones, E. A. Hendrickson for the CV-1 cell line and SV40, M. L. DePamphilis for discussion, A. Landy for critical reading of the manuscript, and E. A. Hendrickson, Z. Han, and members of our laboratory for fruitful discussions. Supported by NIH grant GM 35929.

17 September 1997; accepted 13 November 1997

Modification of the NADH of the Isoniazid Target (InhA) from *Mycobacterium tuberculosis*

Denise A. Rozwarski, Gregory A. Grant, Derek H. R. Barton, William R. Jacobs Jr., James C. Sacchettini*

The preferred antitubercular drug isoniazid specifically targets a long-chain enoyl-acyl carrier protein reductase (InhA), an enzyme essential for mycolic acid biosynthesis in *Mycobacterium tuberculosis*. Despite the widespread use of this drug for more than 40 years, its precise mode of action has remained obscure. Data from x-ray crystallography and mass spectrometry reveal that the mechanism of isoniazid action against InhA is covalent attachment of the activated form of the drug to the nicotinamide ring of nicotinamide adenine dinucleotide bound within the active site of InhA.

Mycobacterium tuberculosis is particularly susceptible to isoniazid [isonicotinic acid hydrazide (INH)], the most widely used of all antitubercular drugs (*1*). Although isoniazid-based treatment regimens have been available since the 1950s, *M. tuberculosis* remains the leading cause of death worldwide from an infectious agent (*2*). Tuberculosis is now a disease associated with poverty and with acquired immunodeficiency syndrome (AIDS); the greatest impact is experienced in underdeveloped nations and in centers of urban decay (*3*). In addition, the incidence of incurable cases due to multidrug-resistant mutants is on the rise. These trends have generated renewed interest in elucidating the molecular mechanisms of action of well-established antitubercular drugs as an aid in